Journal of Applied Mechanics and Technical Physics, Vol. 40, No. 6, 1999

THE FLOW IN A PLANAR-RADIAL VORTEX CHAMBER. 1. AN EXPERIMENTAL STUDY OF THE VELOCITY FIELD IN TRANSIENT AND STEADY FLOWS

F. A. Bykovskii and E. F. Vedernikov

UDC 533.608

Two methods for determining the flow velocity in a vortex chamber of planar-radial geometry under transient and steady-state conditions are proposed. Local flow velocities throughout the entire volume of the chamber are measured, and the flow is found to be rotational. The effect of accumulation of particles heavier than air in the butt-end boundary layer is revealed.

In [1, 2], self-ignition of fuel mixtures is described which is observed in vortex chambers of planar-radial geometry whose diameter is much greater than the height ($d_{ch} \gg Z$). The mechanism of self-ignition remained unclear, and, therefore, it became necessary to determine the flow parameters, in particular, the flow-velocity field in vortex chambers of such geometry. Both reported theoretical studies [3, 4] and experimental methods [5, 6] cannot help in determining the flow velocity with allowance for compressibility, especially under transient conditions. In the present paper, new methods for determining the flow velocity under steady-state and transient conditions are proposed. A direct method in which the velocity is measured by observing tracks of radiating particles and an indirect method based on measurement of temperature and stagnation and static pressures are used.

1. Vortex Chamber and Experimental Setup. The diagram of the chamber and experimental setup is shown in Fig. 1. The vortex channel is a semiclosed volume bounded by flat horizontal walls with a gap $Z = 15$ mm, and a cylindrical surface of diameter $d_{ch} = 204$ mm. One of the radial walls was made of steel and had an outlet of diameter $d = 40$ mm, and the other wall was made of acrylic plastic. In the cylindrical surface, 3 mm away from the transparent wall, 300 equally spaced holes 1.2×0.5 mm were provided at an angle 30° to the tangent line. Steady injection of air through the holes was ensured by a collector whose cross-sectional area was 2.2 times greater than that of the holes. The air was fed into chamber 1 from receiver 2 through valves 3, whose actuation time did not exceed 1 msec. The volume of the receiver V_r was 3.6 liters. In some tests, to obtain a steady flow, we used a 80-liter receiver. The initial pressure of air in all tests was $100 \cdot 10^5$ Pa. It was registered by manometer 4. The moment of full emptying of the receiver was registered by pressure gauge 5.

The volume of the collector through which the air was ejected out of the receiver into the chamber was comparable with that of the chamber: 0.3 and 0.5 liters, respectively. Therefore, under transient conditions, the collector was also filled by air, and the rate of air discharge into the chamber increased from zero to a certain maximum value, and then it began to decrease as the receiver got emptied. According to our estimates based on pressure measurements in the collector and on consideration of the conditions of supercritical ejection through the holes, the air mass-flow rate amounted roughly to 2 kg/sec by the moment 10 μsec. At the same

Lavrent'ev Institute of Hydrodynamics, Siberian Division, Russian Academy of Sciences, Novosibirsk 630090. Translated from Prikladnaya Mekhanika i Tekhnicheskaya Fizika, Vol. 40, No. 6, pp. 112–121, November–December, 1999. Original article submitted March 10, 1998; revision submitted December 3, 1998.

0021-8944/99/4006-1097 $22.00

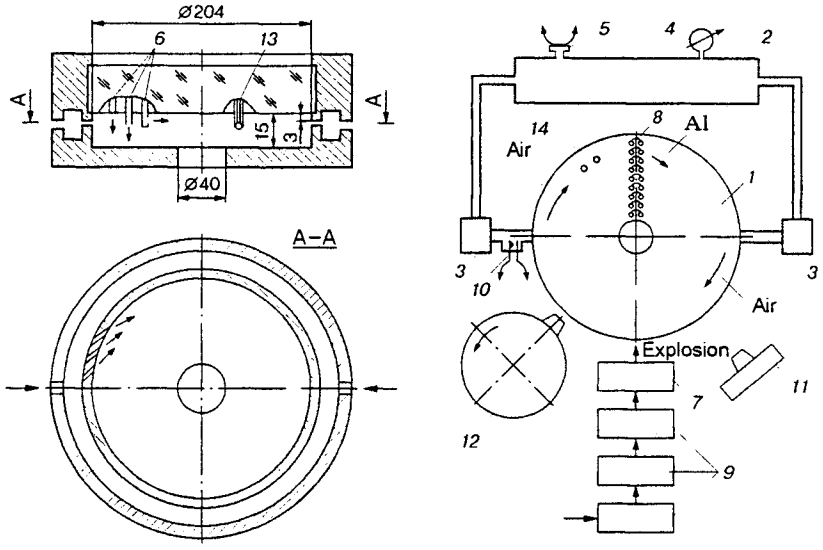

Fig. 1. Diagram of the experimental chamber and setup: 1) chamber; 2) receiver; 3) valves; 4) manometer; 5) pressure gauge; 6) channels for injecting aluminum particles; 7) assembly for exploding foil strips; 8) foil strips; 9) oscillographs; 10) contact gauge; 11) camera; 12) photorecorder; 13) thermocouple; 14) pockets for pressure gauges.

time, the air mass-flow rate from the receiver estimated from the measured pressure in it [7] was twice as high.

2. Local Flow-Velocity Measurement with the Help of Tracks. The tracks were produced by injection into the air flow of explosion products of aluminum-foil strips fused with electric current. The 3 mm-long strips had the cross-sectional area 0.05 × (0.3–0.4) mm. Entering the flow, the aluminum particles were entrained by air, and started burning and emitting light. To reduce the sideway spread of explosion products and avoid unintentional introduction of obstacles for the flow, the foil strips were inserted into channels of chamber wall 6 by 6 mm. In some tests, a plastic tube was inserted into each channel to organize the injection of explosion products at different distances from the wall. In some cases, the tube was soldered and the products were injected along the chamber plane through a side hole 0.5 mm in diameter (Fig. 1).

The foil strips were exploded by discharging an electric capacitor with a capacity of 10^{-2} F charged to a voltage of 46 V with a classical electric circuit [8]. For each foil strip to be exploded, an individual discharge circuit was composed. All the circuits were contained in one assembly 7. To cover the flow along the chamber radius to the largest possible extent, nine foil strips 8 to be exploded were installed 20, 30, 40, 50, 60, 70, 80, 91, and 98 mm away from the center of the chamber. The moment of time at which the electric pulses were fed to the strips was set by three oscillographs 9 triggered by contact gauge 10 upon the origination of flow in the inlet pipe.

The radiating aluminum particles were photographed by camera 11 with an open shutter and, simultaneously, by drum photorecorder 12 with a film moving along the circumference with a velocity of 100 m/sec (Fig. 1). In the stationary film, the tracks of the particles were recorded from the moment of their injection into the flow to their full combustion or escape from the chamber (Fig. 2a), while the moving film was used to trace the track evolution in time (Fig. 2b). For clarity, the images obtained for only one strip are shown. When all nine strips were exploded, the resulting picture, although being too crowded, was quite suitable for analysis. Nontransparent strips glued along the radii and separated by angles $\Delta\alpha = 22.5°$ are shown in Fig. 2a. In the photograph (Fig. 2b), these strips interrupted the particle glow, thus, making it possible to determine the coordinates of each particle at a certain moment of time. The horizontal strips did not register the radial position of the particles, but produced a convenient horizontal reference line on the photograph.

Figure 2a allows one, using the starting segment of particle tracks, to plot an instantaneous air stream-

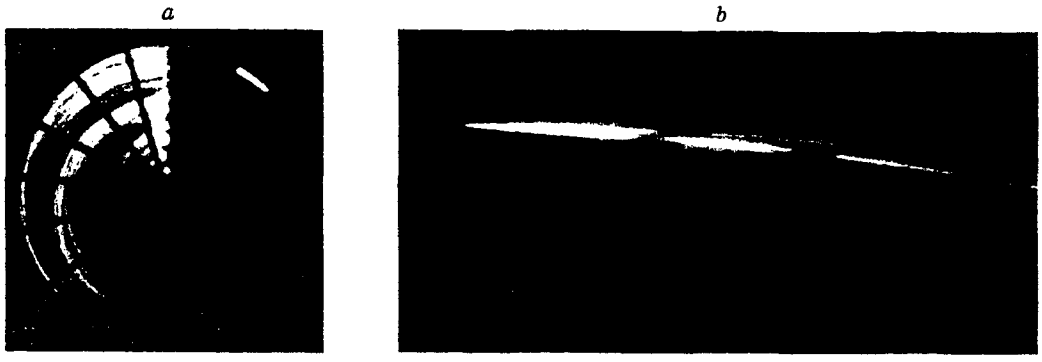

Fig. 2. Tracks of burning aluminum particles: (a) in the stationary film; (b) in the moving film (for one and the same foil strip).

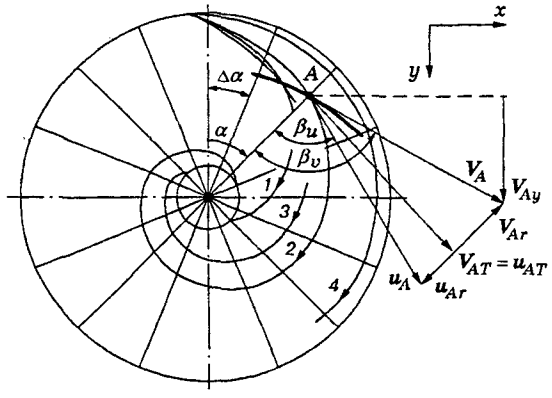

Fig. 3. Streamlines at $t = 10$ msec in the butt-end boundary layer (1) and the flow core (2–4).

line, which passes through the point where the particle was injected into the flow, since after the injection the particle moves along the local velocity of the air flow, or, more accurately, along the tangent direction to the streamline. Afterwards, centrifugal forces and frictional forces of the medium start acting upon the burning particles, and, under their action, separation of particles according to their density occurs: particles lighter than air move toward the center, while heavy particles move toward the periphery. In many cases, the particle beam was diverging and the streamline direction was found by averaging track directions in the beam.

The accuracy of geometric reconstructing of the streamline from the directions of local flow velocities depended on the smoothness of joining individual segments of the streamline. The most exact alignment was achieved when the tangent lines met at the middle of the sector bounded by the radii through which two neighboring tangent lines passed (Fig. 3). The directions of the velocities along different streamlines and their values were transposed along the radius to one streamline that crosses many radii of the chamber. This procedure is justified if the parameters of the air flow along the cylindrical surfaces of an equal radius at a fixed height in the chamber are identical. The above is the case (if possible fluctuations of the parameters are ignored) because of the axial symmetry of both the chamber and the air supply through a great number of holes equally spaced around the cylindrical surface.

Figure 3 shows several streamlines (a part of aluminum-particle trajectory is shown with a bold segment). To derive formulas by which the local flow velocity along the streamlines were reconstructed, e.g., the velocity along line 2, we take the intersection point of a particle track with a nontransparent strip from the image recorded in the moving film and transpose it onto the streamline with the same radial coordinate

(point A in Fig. 3; see also Fig. 2b). This can be done due to axial symmetry of the flow. Decomposition of the particle velocity $\boldsymbol{V}_A$ and the flow velocity $\boldsymbol{u}_A$ into two components, circumferential ($\boldsymbol{V}_{AT}$ and $\boldsymbol{u}_{AT}$) and radial ($\boldsymbol{V}_{Ar}$ and $\boldsymbol{u}_{Ar}$), shows that, to determine the flow velocity $\boldsymbol{u}_A$, it is required to determine the particle velocity $\boldsymbol{V}_A$ and employ the condition of equality of the circumferential velocities: $\boldsymbol{V}_{AT} = \boldsymbol{u}_{AT}$. This condition also follows from the solution of differential equations of the radial and circumferential motion of particles in the chamber.

Using the equation of radial motion of the particle $F_r - F_c = ma_r$, we perform the substitutions

$$mV_T^2/r - C_D\rho_u[(V_r - u_r)^2/2]\pi D^2/4 = m\,dV_r/dt$$

or

$$\rho_v\pi D^3/6)V_T^2/r - C_D\rho_u[(V_r - u_r)^2/2]\pi D^2/4 = (\rho_v\pi D^3/6)\,dV_r/dt.$$

Finally, we obtain $D = (3/4)(\rho_u/\rho_v)C_D(V_r - u_r)^2/(V_T^2/r - dV_r/dt)$, where F_r and F_c are the centrifugal and drag forces, a_r and m are the normal acceleration and mass of the particle, ρ_u and ρ_v are the air and aluminum densities, respectively, D is the particle diameter, C_D is the drag coefficient caused by the flow, and r is the radial coordinate of the particle.

Now we restrict our consideration to the estimate of the size of an individual particle from the data taken from flow calculations. For $r = 65$ mm, $\rho_u = 52$ kg/m^3, $\rho_v = 2.7 \cdot 10^3$ kg/m^3, $V_r - u_r = 16$ m/sec, $V_T = 158$ m/sec, $\Delta V_r = 8$ m/sec, $\Delta t = 10^{-4}$ sec, and $C_D = 0.4$, for the Reynolds number $\mathrm{Re} = 3 \cdot 10^3$, we obtain $D = 4.8$ μm. Tracing the motion of the particle in the chamber, from the data on variation of the particle diameter, we can also determine the degree of its burning-out.

Using the equation of circumferential motion of the particle $F_c = m\,dV_T/dt$ or $C_D\rho_u[(V_T - u_T)^2/2]\pi D^2/4 = (\rho_v\pi D^3/6)\,dV_T/dt$, we obtain $(V_T - u_T)^2 = (4/3)(\rho_v/\rho_u)(D/C_D) \times dV_T/dt$. Denoting $V_T - u_T = \Delta V_T$, solving the differential equation, and assuming that $\Delta V_T = -158$ m/sec for $t = 0$, we have $-\Delta V_T = 1/(1.2 \cdot 10^3 t - 0.0063)$. Already at $t = 0.2$ msec, the difference between the particle velocity and the local velocity of the flow amounts to 4 m/sec, which is well within the largest possible error of velocity measurements. Thus, the adopted condition $V_T = u_T$ is justified.

From Fig. 3 it follows that $y = ky'$, $V_{Ay} = V'k(\Delta y'/\Delta x')/[1 \pm (\Delta y'/\Delta x')\tan(\pm\beta_v \mp \alpha)]$, $V_A = V_{Ay}/\cos(\beta_v - \alpha)$, $V_{AT} = V_A\cos(90^\circ - \beta_v)$, $V_{Ar} = V_A\sin(90^\circ - \beta_v)$, $u_{AT} = V_{AT}$, $u_A = u_{AT}/\cos(90^\circ - \beta_u)$, and $u_{Ar} = u_A\cos\beta_u$, where V_{Ay} is the vertical velocity of the particle, k is the reduction coefficient of the photo, y is the radial coordinate of the point A in the chamber at the corresponding radius, $\Delta y'$ and $\Delta x'$ are the increments of the coordinates of the particle image recorded on the moving film at the point A, $V' = 100$ m/sec is the velocity of the film motion, β_v and β_u are the angles between the radius and the tangent line to the particle track and the streamline, and α is the angular position of the point A.

In the formula for V_{Ay}, the upper plus and minus correspond, respectively, to compensation, when the direction of the film motion coincides with the direction of the velocity of the particle image, and to the lower decompensation, when these directions are opposite. To determine the velocity along the streamline, one must have a sufficient number of intersection points of the streamline with particle tracks. Sometimes, it suffices to trace the trajectory of just one particle from the periphery of the chamber to its center.

The above-considered method is applicable in full measure to determine the direction of the local flow velocity at the point of particle injection into the flow, and, when there is a sufficient number of such points, one can reconstruct an instantaneous streamline along the chamber plane, including the region of the butt-end boundary layer. This method works well when applied to velocity fields uniform throughout the entire height of the chamber and to the so-called *total* velocity field in the flow core. In the case of a *non-total* velocity field and in the case of a boundary layer, it is unclear at which distance from the flat wall the aluminum particle is located. This uncertainty exists when the directions of local flow velocities are the same throughout the entire height of the chamber. Injecting particles into the flow through the side hole of tube 6 (see Fig. 1), it is possible to make the particle position definite and find the local velocities in all velocity fields, even in the butt-end boundary layer. However, in the case of developed turbulence, the uncertainty still exists since the particles diverge along the channel height.

The method introduces some errors when applied to local velocity measurement caused by flow unsteadiness, since the velocity measurement along particle tracks in this method is performed 0.2–1.0 msec after the injection of particles into the flow. This error can be estimated and allowed for if the information on the radial distribution of the angles β_u in the flow core and in the butt-end boundary layer during the transient process is available.

The use of tubes for injection of aluminum particles seems to be undesirable since the tubes distort the flow pattern. From this point of view, most suitable is the injection of particles into the flow core through a hole in the wall, but in this case there arises a question on the penetrating power of the jet of particles, namely: Do the particles really get through the boundary layer and reach the flow core or not? To answer this question, we carried out special tests and performed some estimates of the propagation range of the jet using the differential equation $F_c = ma_z$, where a_z is the acceleration of the particle along the chamber height. For $\rho_u = 40$ kg/m^3, $D = 5$ μm, and initial velocity of the injected particle jet 100 m/sec determined from the images recorded on the moving film by estimating the time interval between the foil explosion and particle injection into the flow, in 0.1 msec the jet travels a distance as large as 5 mm. Therefore, the considered methods of organizing particle injection into the flow seem to be equally convenient.

3. Determination of the Local Flow Velocity from the Measured Temperature and Stagnation and Static Pressures. The method for measuring the stagnation pressure P_0 and static pressure P is described in [9]. The flow was assumed isentropic, and from the known ratio P/P_0, the quantities $\mathrm{M} = u/a$, T/T_0, and ρ/ρ_0 were determined, where M is the Mach number of the flow, a is the velocity of sound, T and T_0 are the static and stagnation temperatures of the flow, and ρ and ρ_0 are the local static and stagnation densities of the flowing medium. The measurement of T_0 and the equation of state $RT_0 = P_0/\rho_0$ permit determination of a, u, ρ_0, and ρ. From the angles β_u measured from track observations, the values of u_T and u_r were determined. The time dependences P_0 and P in the oscillograms showed insignificant fluctuations, which in this work were averaged so that all other parameters derived from them were considered as mean parameters.

Since the temperature was measured under transient conditions, it is required to estimate the resolution of thermocouples. It is known that, in a flow around bodies with high thermal conductivity, the heating of the bodies depends predominantly on the heat exchange with the gas. For the thermocouple to "trace" the local flow temperature, its heating must be the same as possible local gas cooling in the boundary layer: $q_{\mathrm{th}} \approx q_{\mathrm{gas}}$. For the case of a thermocouple in the form of a thin plate, we have $c\delta S\rho\Delta T \approx \alpha_{\mathrm{gas}} 2S\Delta T\Delta t = (\mathrm{Nu}\,\lambda/\delta)2S\Delta T\Delta t$, from which it follows that the thermocouple thickness δ must be smaller than $\delta = [2\,\mathrm{Nu}\,\lambda\Delta t/(c\rho)]^{0.5}$, where $c \approx 10^3$ J/(kg·deg), $\lambda \approx 4 \cdot 10^{-2}$ J/(m·sec·deg), and $\rho \approx 8 \cdot 10^3$ kg/m^3 are the mean heat capacity, thermal conductivity, and density of the thermocouple, respectively, S is the area of the side surface, ΔT is the change in the thermocouple and gas temperatures, α_{gas} is the heat-transfer coefficient, $\mathrm{Nu} = AR^m\mathrm{Pr}^n K_t$ is the Nusselt number, Δt is the typical time of local flow-temperature variations (resolution of the thermocouple), $K_t = (T_{\mathrm{gas}}/T_{\mathrm{th}})^{0.5}$ is the intermittency coefficient of gas properties, and T_{gas} and T_{th} are the gas and thermocouple temperatures. For a flow with Reynolds number $\mathrm{Re} \approx 10^4$, Prandtl number $\mathrm{Pr} \approx 0.72$, $A = 0.023$, $m = 0.8$, $n = 0.4$, and $T_{\mathrm{gas}} = T_{\mathrm{th}}$ [10], we have $\mathrm{Nu} \approx 30$. For $\Delta t = 10^{-4}$ sec (characteristic time of the half-period of flow oscillations [9]), the thickness of the thermocouple should not exceed 5.5 μm. Under transient conditions with duration of about 30 msec, $\Delta t \approx 1$ msec, and, therefore, the thickness of the thermocouple should not exceed 17.5 μm. The length of the thermocouple from the junction between its components (Chromel and Alumel) should exceed, or be equal to, the characteristic depth of metal heating, $x = (a_{\mathrm{th}}t)^{0.5}$, where $a_{\mathrm{th}} \approx 10^{-6}$ m^2/sec is the temperature diffusivity of the thermocouple. For $\Delta t = 10^{-4}$ sec and $\Delta t = 10^{-3}$ sec, we have $x \approx 10$ μm and $x \approx 30$ μm, respectively. The width of the thermocouple is of no significance (if the temperature gradient along it is ignored) and can be chosen from the viewpoint of convenience of its fabrication or from strength considerations.

The thermocouple used in this work was made in the form of a thin plate of thickness $\delta = 5$ μm or

$\delta = 20$ μm, width about 0.5 mm, and length about 1 mm. The side surfaces of the plate smoothly transformed into a wire 0.3 mm in diameter and were glued into a tube 2 mm in diameter. The Chromel–Alumel wires were welded together by a special technology, and the desired thickness of the working part of the thermocouple was attained by riveting the welded part in a special fixture. Calibration of the thermocouple in boiling water showed good agreement with the standard characteristic: 4.1 mV per 100°C [11]. Thermocouple 13 was mounted in pockets 14 intended for pressure gauges (see Fig. 1) and could measure the temperature profile throughout the entire height of the chamber from one wall to another.

Installing the thermocouple plate parallel to the flow, we measured the stagnation temperature $T_0 = T + \sigma u^2/(2c_p) = T + \sigma(\gamma - 1)/(2\mathrm{M})$, where σ is the coefficient of stagnation-temperature recovery [12, 13], c_p is the specific heat of air at constant pressure, and γ is the ratio of specific heats. For the actual parameters of the flow, $\sigma \approx \mathrm{Pr}^{0.5} = 0.85$. In the tests, somewhat lower values of T_0 were obtained, the deviation being smaller than 2.5%.

4. Measurement Results and Their Discussion. The instantaneous streamlines reconstructed from the measured flow-deflection angles β_u are shown in Fig. 3. In this figure, streamline 1 corresponds to the butt-end boundary layer and streamlines 2–4 to the flow core for $t = 10$ msec. Streamline 2 is reconstructed using the mean values of the angle β_u; it is a combination of two Archimedean spirals in the flow regions $r < (2/3)R$ and $r > (2/3)R$, where R is the chamber radius. Streamlines 3 and 4 are the extreme positions of the flow streamlines which correspond to varying flow modes under transient conditions.

The time evolution of the angles β_u and their distributions over the chamber radius and height were studied using the injection of aluminum particles through tubes immersed into the flow. It was found that β_u changes dramatically at a distance of 1–1.5 mm from the wall. The drastic change in β_u near the wall confirms the data of [14] on the presence of two flow regions: in the flow core and in the butt-end boundary layer. The flow in the butt-end boundary layer was studied in detail by Volchkov et al. [15].

The angles β_u in the transient regime were found to change significantly both in the flow core and in the butt-end boundary layer. In the flow core, in the region $r < (2/3)R$, within the time interval $t < 20$ msec during which the flow was most unstable, the angles β_u varied only slightly, within $(85 \pm 5)°$. In the region $r > (2/3)R$, the value of β_u varied in the range $(80 \pm 10)°$, and the transition from $\beta_u = 90°$ to $\beta_u = 70°$ occurs in tenth parts of a millisecond. This estimate was made by analyzing the spread of β_v during the time of particle injection, which was sometimes as long as 0.5 msec, and the inflections of the beam of particle tracks during the flow evolution in the chamber. The flow with $\beta_u > 80°$ is the most long-lived. After $t = 20$ msec, the flow becomes more stable, and at $t = 300$ msec, the value of β_u equals $(82 \pm 3)°$ in the region $r > (2/3)R$ and $(80 \pm 3)°$ in the region $r < (2/3)R$.

Variation of β_u with time in the butt-end boundary layer for points $r = 40$, 60, and 80 mm is shown in Fig. 4. The dashed curves show the limiting values of β_u in the flow core. Since, in this case, the gas flew out of the receiver of volume $V_\mathrm{r} = 3.6$ liters, the air flow was not perfectly stable because of the gradual variation (decreasing) of the air-supply parameters P_0, T_0, and ρ_0. The angles β_u show considerable changes at $t < 20$ msec. Here, the difference in β_u for the flow core and for the side boundary layer is maximum, except for the moments of drastic reconstruction of the flow at which the angles in both flows become closer. After the time $t = 20$ msec, the angles are stabilized and the difference in the angles for the core flow and the butt-end boundary layer decreases at the periphery. Near the periphery, the angles are practically the same, and in the vicinity of the chamber outlet, the two flow patterns are quite stable. The values of β_u for $r = 80$, 60, and 40 mm (points A, B, and C, respectively) in the butt-end boundary layer for the steady flow ($V_\mathrm{r} = 80$ liters) are shown in Fig. 4. The difference in β_u for the butt-end boundary layer and for the flow core is retained throughout the entire flow. The angles β_u in the side boundary layer were measured only near the wall opposite to the outlet. Near the other wall, their values may differ.

The profiles of the local flow velocity under transient ($t = 9.5$ msec) and steady conditions ($t = 100$ msec) along the radius r and the chamber axis z are shown in Fig. 5. Variation of the local flow velocity with time in the butt-end boundary layer ($z = 0.5$ mm) for $r = 80$ mm and $r = 40$ mm is shown in Fig. 6.

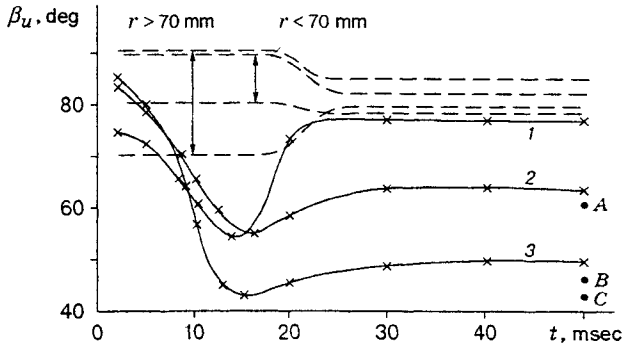

Fig. 4. Variation of β_u in time in the butt-end boundary layer (solid curves) and the range of β_u in the flow core (dashed curves) (V_r = 3.6 liters) for r = 80 (1), 60 (2), and 40 mm (3); filled points refer to a steady flow (V_r = 80 liters) for r = 80 (A), 60 (B), and 40 mm (C) (crosses refer to experimental data).

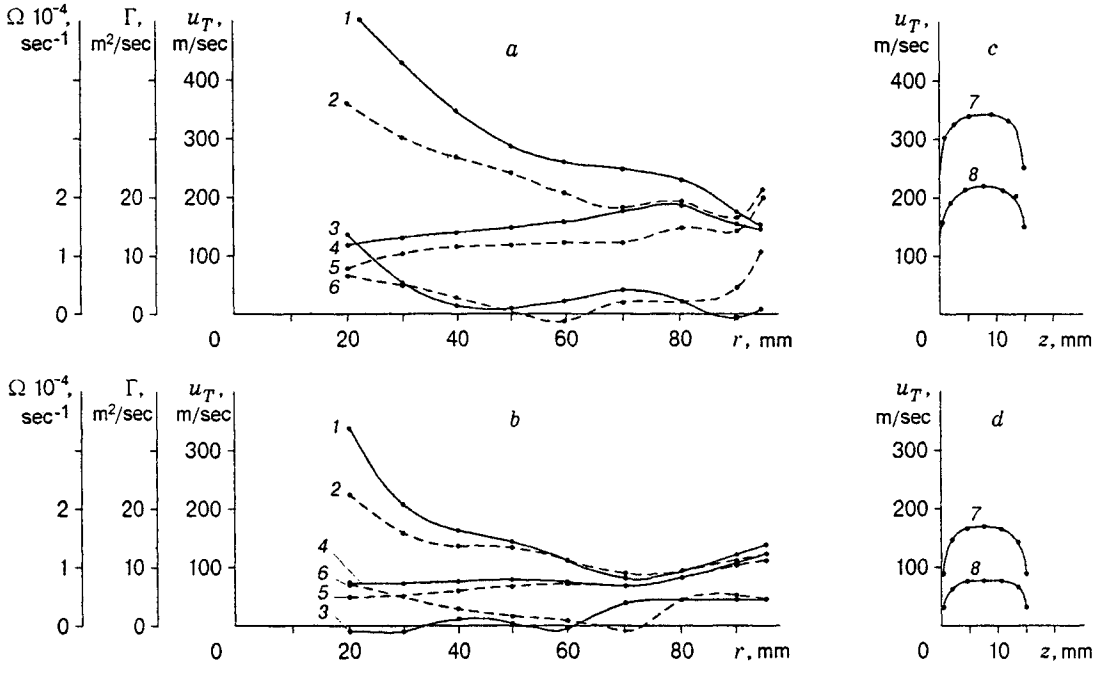

Fig. 5. Vorticity, circulation, and flow velocity profiles along the chamber radius in the transient (a and c) and steady (b and d) flows: (a) t = 9.5 msec, z = 7.5 mm, and V_r = 3.6 liters; (b) t = 100 msec, z = 7.5 mm, and V_r = 80 liters; (c) t = 9.5 msec and V_r = 3.6 liters; (d) t = 100 msec and V_r = 80 liters; solid and dashed curves denote the second and first methods, respectively; curve 1 refers to u_T^f, 2 to u_T^{tr}, 3 to Ω^f, 4 to Γ^f, 5 to Γ^{tr}, and 6 to Ω^{tr}, and curves 7 and 8 refer to r = 80 and 40 mm, respectively (points refer to experimental data).

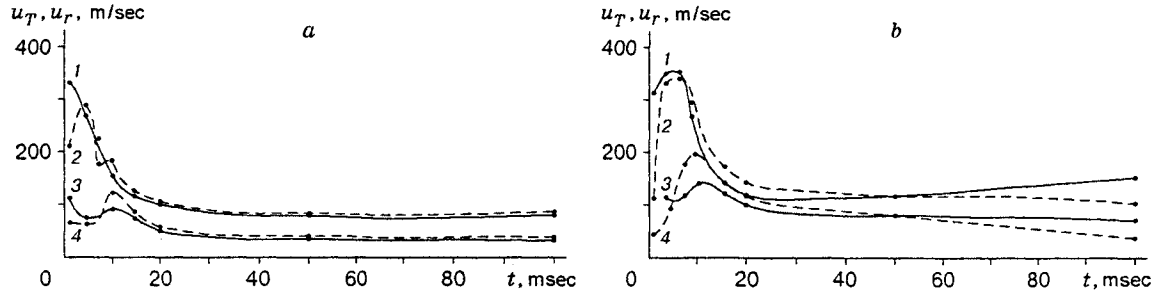

Fig. 6. Variation of flow velocities in time in the butt-end boundary layer ($z = 0.5$ mm and $V_r = 3.6$ liters) for $r = 80$ (a) and 40 mm (b); solid and dashed curves denote the second and the first methods, respectively; curve 1 refers to u_T^f, 2 to u_T^{tr}, 3 to u_r^{tr}, and 4 to u_r^f (points refer to experimental data).

The presented values of the local flow velocity were obtained by two methods: by the first method based on the observation of particle tracks and by the second method based on the measurement of flow parameters. The second method was believed to be more reliable, since the positions of the gauges in the flow were known with good accuracy. In the track method, the exact position of the radiating aluminum particles along the chamber axis was unknown except for the moment when the particles were injected into the flow, and, therefore, the velocities measured by this technique were compared with the velocities calculated by the second method. The comparison was performed in terms of the tangent velocities (u_T^f and u_T^{tr}), since these velocity components u_T^{tr} were determined with better accuracy in the track method.

From Fig. 5, it is seen that, for $t = 9.5$ msec and $z = 7.5$ mm, the two velocities are almost equal only at the periphery of the chamber. For other moments of the transient processes, the velocities exhibit nearly the same radial distributions. Under steady-state conditions, the width of the region where the two velocities are almost equal increases to $r = 60$ mm. For smaller radius, the difference between these velocities increases, and $u_T^f > u_T^{tr}$. Along the chamber axis z (the z-axis is directed toward the outlet) $u_T^f \approx u_T^{tr}$ in the butt-end boundary layer. The difference between the two velocities decreases during the whole transient process (see Fig. 6) and after reaching the steady state of the flow ($V_r = 80$ liters).

The above results indicate that, alongside with the separation of aluminum particles along the chamber radius, their accumulation takes place in the butt-end boundary layer. Inside this boundary layer, the heavy particles penetrate into the region with the lowest tangent flow velocity. Figure 6 shows that, in the region $r < (2/3)R$ ($r = 40$ mm), these particles accumulate with time ($t > 50$ msec) in the 0.5 mm-thick near-wall region. In the steady flow, in the region $r > (2/3)R$, no accumulation of particles inside the boundary layer is observed because of the developed large-scale flow turbulence [9], and the track method registers velocities characteristic of the both flow regions.

The possible reason for the above accumulation of aluminum particles is the Magnus forces arising in the viscous flow around rotating particles, which occurs in the case of developed turbulence. The angular-velocity vector can be arbitrarily directed, and, being injected into the flow, the particles move randomly. Entering the butt-end boundary layer, where the turbulence decays and the dissipation of the rotational energy of particles occurs, the particles do not escape from this layer. The concentration of the particles in the butt-end boundary layer increases by tenths of a millisecond after particle injection into the flow.

The radial velocities of the air in the flow core are low and amount to only 15% of u_T. Their values increase with decreasing chamber radius r. In the butt-end boundary layer, they are quite comparable with u_T and increase with decreasing r (see Fig. 6).

The transient flow, as judged from the values of circulation $\Gamma = u_T r$ and vorticity $\Omega = u_T/r + \partial u_T/\partial r$, is rotational throughout the whole chamber (see Fig. 5). The vorticity is especially pronounced at the periphery of the chamber and near the chamber outlet. In the steady regime, the vorticity in the flow core remains in the region $r > (2/3)R$. The flow formed here resembles the rotational motion of a solid body. In the

region $r < (2/3)R$, we have $\Gamma \approx$ const and $\Omega \approx 0$, and a flow that resembles the flow in a potential vortex is observed. In the butt-end boundary layer, the value of Ω remains constant throughout the entire chamber radius.

5. Conclusions. (1) New methods for local flow velocity measurement in the planar-radial vortex chamber under steady-state and transient conditions are proposed: one method is based on the observation of tracks of aluminum particles burning in air, and the second method is based on temperature, stagnation-pressure, and total-pressure measurements.

(2) Experimental evidence is obtained for the occurrence of two flow regions, in the flow core and in the butt-end boundary layer. The directions of flows in both regions are measured for steady-state and transient flows.

(3) The transient flow is rotational throughout the whole chamber. Under steady-state conditions, in the core of the flow, between the chamber periphery and two-thirds of the chamber radius, the flow resembles the revolution of a quasi-solid body, and in the region between the chamber outlet and the above region, the flow is close to the flow in a potential vortex.

(4) Particles heavier than air (e.g., burning aluminum particles) are found to accumulate in the butt-end boundary layer.

This work was supported by the Russian Foundation for Fundamental Research (Grant No. 96-02-19121a).

REFERENCES

1. F. A. Bykovskii, V. V. Mitrofanov, and E. F. Vedernikov, "Autoignition in rotational flow of combustible mixture," in: *Proc. of the 16th Int. Conf. on the Dynamics of Explosions and Reactive Systems*, Univ. of Mining and Metallurgy, Cracow, Poland (1997), pp. 297–298.
2. F. A. Bykovskii, V. V. Mitrofanov, and E. F. Vedernikov, "Self-ignition in gas-mixture flows," *Dokl. Ross. Akad. Nauk*, **358**, No. 4, 487–489 (1998).
3. M. A. Gol'dshtik, "On the theory of the Ranque effect (swirling flow of a gas in a vortex chamber)," *Izv. Akad. Nauk SSSR, Otd. Tekh. Nauk*, **1**, 132–137 (1963).
4. A. V. Lebedev and M. Kh. Pravdina, "A model of planar flow in a vortex chamber. 2. Turbulent viscosity in a peripheral region," *Teplofiz. Aéromekh.*, **3**, No. 4, 317–320 (1996).
5. É. P. Volchkov, A. P. Kardash, and V. I. Terekhov, "Fluid dynamics in a vortex chamber with hyperbolic butt-end lids," *Izv. Sib. Otd. Akad. Nauk SSSR, Ser. Tekh. Nauk*, **13**, No. 3, 33–41 (1981).
6. A. V. Lebedev and M. Kh. Pravdina, "An experimental study of the pressure in the near-axial region of the vortex chamber," *Teplofiz. Aéromekh.*, **2**, No. 1, 21–27 (1995).
7. F. A. Bykovskii and E. F. Vedernikov, "Discharge coefficients of nozzles and of their combinations in forward and reverse flows," *Prikl. Mehk. Tekh. Fiz.*, **37**, No. 4, 98–104 (1996).
8. W. G. Chase and H. K. Moore (eds.), *Exploding Wires*, Chapman and Hall, London (1959).
9. F. A. Bykovskii and E. F. Vedernikov, "Flow in a vortex planar-radial chamber. 2. Vortex flow structure," *Prikl. Mekh. Tekh. Fiz.* (in press).
10. M. Barrere, A. Jaumotte, B. F. Veubeke, and J. Vandenkerckhove, *Rocket Propulsion*, Elsevier, Amsterdam–London–New–York–Princeton (1960).
11. A. M. Turichin, *Electrical Measurements of Non-Electrical Quantities* [in Russian], Gosenergoizdat, Moscow (1959).
12. G. Schlichting, *Boundary Layer Theory*, McGraw-Hill, New York (1968).
13. A. I. Borisenko, *Fluid Dynamics of Engines* [in Russian], Oborongiz, Moscow (1962).
14. M. A. Gol'dshtik, *Vortex Flows* [in Russian], Nauka, Novosibirsk (1981).
15. É. P. Volchkov, S. S. Semenov, and V. I. Terekhov, "Butt-end boundary layer in the vortex chamber," in: *Structure of Forced and Thermogravitational Flows* (Collected scientific papers) [in Russian], Inst. of Thermal Physics, Sib. Div., Acad. of Sci. of the USSR (1983), pp. 51–87.